

The Influence of Leading-Edge Tubercles on Wake Flow Dynamics of a Marine Rudder

MARINE 2021

Moritz M. F. Troll^{1,*}, Weichao Shi¹ and Callum Stark¹

¹ Department of Naval Architecture, Ocean and Marine Engineering (NAOME), University of Strathclyde, Henry Dyre Building, 100 Montrose Street, G4 0LZ Glasgow, UK. Email: moritz.troll@strath.ac.uk, web: <https://www.abmhydro.com/>

* Corresponding author: Moritz Troll, moritz.troll@strath.ac.uk

ABSTRACT

The impact of two tubercle leading-edge (TLE) modifications on the turbulent wake of a representative marine rudder at Reynolds number 2.26×10^6 was analysed numerically using Detached-Eddy Simulations. TLE have been shown to alter the flow profile over aero/hydrofoils through the generation of streamwise counter-rotating vortex pairs behind the tubercles, which can enhance the lifting performance. This paper studies the formation of these vortex pairs and their impact on the wake structures behind the rudder to find out if vortex interaction can reduce the tip vortex.

The tubercles enhanced lift for angles of attack (AOA) 10° and above, but at the cost of a large drag penalty that reduced the rudders' lift-to-drag ratio. The formation of the distinctive streamwise counter-rotating vortex pairs behind the tubercles was shown. Due to the inherent spanwise flow component of finite-span lifting surfaces the vortices were generated at unequal strength and only positive vortices were maintained in the wake. The vortices facilitated flow compartmentalisation over the rudder suction side which broke up the trailing-edge vortex sheet and confined the spanwise flow separation over the rudder surface as AOA increased. The tubercles confined flow separation closer to the rudder tip which caused a tip-offloading effect that minimised the initial tip vortex strength. Large elements of streamwise counter-rotating vorticity formed around the localised stall cells of the TLE rudders that interacted with the tip vortex downstream, introducing elliptical instabilities further weakening the tip vortex and changing its trajectory.

Keywords: Rudders, Biomimetic Design; Leading-Edge Tubercles; Computational Fluid Dynamics; Tip Vortex; Vortex Interaction.

NOMENCLATURE

A	Tubercle amplitude [m]
A_{lift}	Lifting area [m ²]
C_D	Drag coefficient [-]
C_L	Lift coefficient [-]
$C_{L\text{max}}$	Maximum lift coefficient [-]
C_n	n^{th} tubercle crest [-]
C_{nom}	Nominal chord length [m]
C_P	Pressure coefficient [-]
D	Drag force [N]
L	Lift force [N]
L_{domain}	Length of the computational domain [m]
M_{11}	11.3 million cell mesh [-]
M_{21}	21.6 million cell mesh [-]
N_i	Mesh cell count [-]
R_n	Reynolds number [-]

S	Span [m]
T_n	n^{th} tubercle trough [-]
V	Free stream velocity [m s^{-1}]
V_{max}	Maximum velocity [m s^{-1}]
y^+	Non-dimensional distance from wall to first mesh node [-]
y_{avg}^+	Average value of y^+ [-]
y_{max}^+	Maximum value of y^+ [-]
α	Angle of attack [deg.]
α_{stall}	Stall angle [deg.]
Δt	Time step [s]
Δ_0	Smallest grid cell length [m]
λ	Tubercle wavelength [m]
ρ	Fluid density [kg m^{-3}]
φ	Critical simulation variable [-]
AR	Aspect Ratio
AOA	Angle of Attack
CFD	Computational Fluid Dynamics
DES	Detached-Eddy Simulation(s)
EFD	Experimental Fluid Dynamics
GCI	Grid Convergence Index
LE	Leading Edge
LES	Large-Eddy Simulation(s)
MCS	Marine Control Surface(s)
RANS	Reynolds-Averaged Navier-Stokes Equations
SA	Spalart-Allamaras
SLE	Straight Leading Edge
SST	Shear Stress Transport
TE	Trailing Edge
TKE	Turbulent Kinetic Energy
TLE	Tubercle Leading Edge

1. INTRODUCTION

The majority of modern ships and submarines use movable control surfaces as their primary steering devices for course keeping and manoeuvring. Most of these marine control surfaces (MCS) are foil-shaped appendages, such as rudders for steering in the horizontal plane, hydroplanes / diving planes for vertical steering on submarines, or fin stabilisers damping roll motions (Molland and Turnock, 2007). They are designed for effectiveness given by the amount of lift that can be generated and for efficiency, reflected in the lift-to-drag ratio (Liu and Hekkenberg, 2017). Whilst essential to the manoeuvring, MCS also contribute to the turbulent wake of a vessel as a result of flow separation on the suction side surface and through the formation of the distinct tip vortices.

In the constant strive to develop MCS that generate higher lift forces, reduced drag forces, and prolong flow attachment to increase the stall angle, researchers recently started drawing inspiration from humpback whales (*Megaptera novaeangliae*). Humpback whale flippers have superior agility amongst baleen whales, which has been attributed to distinctive bumps along their leading edge (LE), the so-called tubercles as shown in Fig. 1.

These tubercles act as passive flow control devices that give the flippers a unique flow profile which prolongs flow attachment, delays stall, and increases post-stall lift (Fish and Battle, 1995; Miklosovic et al., 2007, 2004). Finite span hydro/aerofoils respond particularly well to the addition of TLE. Lift enhancements have been reported in the pre-stall regime and albithe the maximum lift coefficient being reduced there is a more gradual stall behaviour with significant post-stall lift improvements (Custodio et al., 2015; Miklosovic et al., 2007, 2004; Stanway, 2008; Weber et al., 2010). Experimental studies on low aspect ratio (AR) marine rudders with

TLE conducted for NACA 0016 section by Weber *et al.* (2010) and NACA 0018 section by Shanmukha Srinivas *et al.* (2018) reported benefits from tubercles in the post-stall regime. A numerical analysis for marine rudders with NACA 0020 section that had different tubercle coverage along the LE conducted by Yoon *et al.* (2011) also reported superior post-stall performance.



Figure 1. Leading-edge tubercles as seen on a humpback whale pectoral flipper (©Grant Thomas).

These performance improvements from tubercle leading edges (TLE) are widely attributed to the formation of streamwise counter-rotating vortex pairs generated between adjacent tubercles that exchange momentum within the boundary layer, energise the flow over the tubercle crests, and confine separation to the tubercle troughs (Fish *et al.*, 2008; Malipeddi *et al.*, 2012; Pedro and Kobayashi, 2008; Rostamzadeh *et al.*, 2017). The effect of the tubercle vortices has been compared to that of wing fences, which minimise spanwise flow and confine flow separation to small localised stall cells, preventing the rapid spread of flow separation (Bolzon *et al.*, 2015; Pedro and Kobayashi, 2008).

The minimisation of spanwise flow is what makes TLE modifications highly applicable to finite span foils, as several adverse effects can be reduced. The spanwise flow component leads to induced drag due to the downwash and gives rise to the formation of tip vortices that are a very distinct feature within the turbulent wake (Molland and Turnock, 2007). Reducing induced drag will increase the lift as well as overall efficiency. The tip vortices are highly turbulent and slow-decaying flow structures. They dissipate energy from the foil causing drag and their low pressure core may give rise to cavitation and flow noise. They can have adverse effects on structures located in the downstream wake such as propulsors, and their long persistence in the flow adds to the undesirable non-acoustic signature of submarines. The significance of the control surface tip vortex structures within the overall wake of a submarine are evident from the flow visualisations of the Joubert BB2 submarine travelling near the free surface presented in Carrica *et al.* (2019). The tip vortex strength, size, decay, and trajectory may be influenced by the tubercle vortices.

In fact, Shi *et al.* (2016) showed diminishing effects on the tip vortex strength and the associated cavitation for a tidal turbine blade with TLE. Johari (2015) reported for tip vortex cavitation to diminish at lower AOA for a tubercle hydrofoil. Bolzon *et al.* (2017) assessed the impact of a single tubercle at the tip of a swept foil. Their study found that for a peak configuration of the tip tubercle the tip vortex strength was increased, whereas the tubercle vortex closest to the tip in a trough configuration reduced the tip vortex strength. Custodio (2012) on the other hand reported that at for angles of attack (AOA) post stall the tip vortex strength downstream of a tubercle foil increased. This however was attributed to the overall increase in lift from the tubercles. The different tip vortex behaviour due to TLE modifications that has been reported is encouraging. The results from Shi *et al.* (2016) are in contrast to Custodio (2012) as a reduction in tip vortex strength was reported, whilst lift was maintained or even enhanced. This suggests that there may be interaction between the tubercle vortex pairs and the tip vortex. Bolzon *et al.* (2017) showed that if the tubercle vortex closest to the foil tip opposes the tip vortex rotational direction the tip vortex is weakened.

Generally, if two counter-rotating or co-rotating vortices are in parallel and within close enough distance for their respective strain fields to become overlapped, they will begin to interact with and influence each other through two-dimensional dynamics and three-dimensional instabilities. The two-dimensional dynamics address the merging mechanisms between two vortices, whereas the three-dimensional instabilities are mechanisms that displace the vortices from their original trajectories into long-wave Crow instabilities, shortwave elliptical instabilities, or a combination of the two (Leweke et al., 2016). In the wake of a TLE foil there is a great potential for various modes of vortex interaction between the tubercle vortices and the tip vortex or the tubercle vortices amongst themselves. Any potential interactions between the tubercle vortices and the tip vortex can have significant effects on the downstream wake dynamics. Knister *et al.* (2020) for example showed how the presence of a weak secondary vortex can lead to the break-up of a strong primary vortex of opposing sign. However, whilst the presence of the tubercle streamwise counter-rotating vortices has been widely reported, their interaction effects in the turbulent wake and with the tip vortex remains largely unstudied.

As shown, previous researchers have presented strong evidence for tubercle modifications enhancing lifting performance. This has been attributed to the formation of streamwise counter-rotating vortex pairs. The vortices have been shown to persist within the wake behind lifting surfaces, however their effect on the wake and especially the tip vortex is largely unstudied. This study aims to further expand on the limited documentation of the tubercle vortex generation mechanism for finite span lifting surfaces and their effect on the downstream wake. The aim is to find out if this wake and the distinctive tip vortices in particular can be minimised when TLE is applied. Such influence could reduce the non-acoustic signature of marine control surfaces on naval vessels such as submarines where detectability is a primary design factor. This aim will be achieved through the application of a tubercle leading edge to the practical case of a marine rudder for fully turbulent flow at high Reynolds number (R_n) using Computational Fluid Dynamics (CFD).

2. REFERENCE RUDDER MODEL AND LEADING-EDGE MODIFICATIONS

2.1 All-Movable Rudder Reference Model

One of the rudder models presented in Folger Whicker and Fehlner (1958) was replicated to allow for experimental validation of the numerical model. The study provides results for a relatively high R_n of up to 3×10^6 where the flow can be regarded as fully turbulent. The reference rudder has a nominal chord length (C_{nom}) of 0.61m, a span (S) of 0.914m resulting in a geometric aspect ratio of 1.5, a quarter chord sweep angle of 11° , a taper ratio of 0.45, and a rounded-off (semi-circular) tip. It has a NACA 0015 foil section. The rudder was chosen because it is representative of not only a typical marine rudder, but also has a strong resemblance of a typical submarine diving plane, such as seen on the Joubert BB2 submarine model, where a reduction of tip vortex generation may be of particular interest.

2.2 Tubercle Design

Two TLE variations of fixed amplitude with two different wavelengths were designed. The tubercles were modelled as a sine function that was subsequently superimposed onto the linear function of the unmodified LE. The amplitude (A) was fixed at 5.0% C_{nom} , which was the best performing amplitude in a preliminary study. The wavelengths (λ) of the two designs were set to 21% C_{nom} and 36% C_{nom} which resulted in $4^{1/4}$ and $7^{1/4}$ tubercles, respectively. The $1/4$ tubercle arises from the LE modification being designed to terminate on a tubercle crest, in order to produce tubercle vorticity opposing the tip vortex rotational direction from the tubercle closest to the rudder tip, as proposed by Bolzon *et al.* (2017). The three different rudder designs are hereinafter referred to as SLE for the straight leading-edge reference model, TLE4 for the $4^{1/4}$ tubercle model, and TLE7 for the $7^{1/4}$ tubercle model herein after. The three models can be seen in Fig. 2.

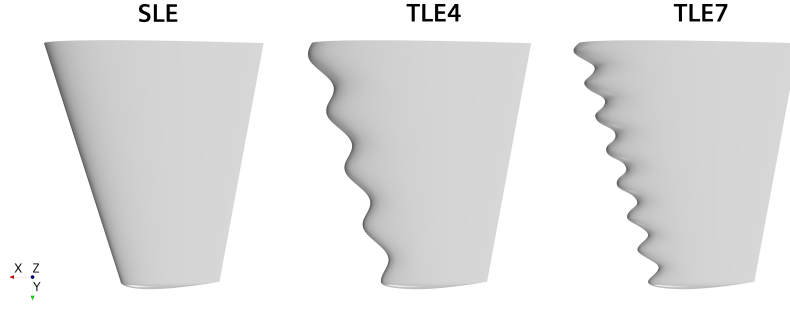


Figure 2. Reference rudder (SLE), 4 tubercle rudder (TLE4), and 7 tubercle rudder (TLE7).

3. NUMERICAL SETUP

3.1 Numerical Model

Analyses were carried out using the commercial Computational Fluid Dynamics (CFD) code STAR-CCM+. The hydrodynamic flow field was solved using Detached-Eddy Simulations (DES). DES is a hybrid approach combining Large-Eddy Simulations (LES) to solve the main fluid domain, whilst Reynolds-Averaged Navier-Stokes (RANS) solvers are used to resolve the near-wall boundary layer flow regions. This approach is highly applicable to the hydrodynamic flow problems targeted in this study due to DES' superior capabilities in resolving the expected separated flow areas without excessive computational requirements. Furthermore, several researchers already presented successful analyses of TLE applications using DES (Câmara and Sousa, 2013; Malipeddi et al., 2012; Pedro and Kobayashi, 2008).

The incompressible segregated SIMPLE flow solver was employed with a hybrid second-order upwind / bounded-central differencing discretisation scheme. Analysing TLE modifications for an infinite span aerofoil in CFD, (Malipeddi et al., 2012) reported the best results for the complex flows at high AOA using DES with the shear stress transport (SST) $k-\omega$ model, whilst stating limitations for the Spalart-Allamaras (SA) model. Early trials as part of this study found similar limitations in the SA model for the stall conditions. Therefore an approach using the Improved Delayed Detached Eddy Simulation (IDDES) solver with the SST $k-\omega$ turbulence model was chosen. Implicit unsteady first-order temporal discretisation was used. The time step (Δt) was calculated following the guidelines by Spalart (2001) shown in Eq. (1)

$$\Delta t = \Delta_0 / V_{\max} \approx 0.001s, \quad (1)$$

where Δ_0 is the smallest grid cell length and V_{\max} is an estimate of the maximum velocity encountered within the flow regions of interest. The mean flow residence time at the target velocity was calculated by Eq. (2)

$$L_{\text{domain}}/V = 2.7s, \quad (2)$$

where L_{domain} is the length of the computational domain and V is the freestream velocity. Solution times of twice the residence time around 6.0 seconds were targeted for the flow to achieve statistical steadiness and to allow for time-averaged results to be taken.

3.2 Computational Domain and Boundary Conditions

A cuboid-shaped domain was created with the rudder placed vertically centred on the right-hand-side boundary (see Fig. 3). The coordinate origin was located at the rudder stock location on the root chord, with the x-axis in the upstream, y-axis in the span, and z-axis in the vertical direction. The velocity inlet was placed 5 chord lengths upstream, the pressure outlet 15 chord lengths downstream, the top, bottom, and left-hand-side boundaries were set to be slip walls and placed 5 chord lengths from the origin each. No interference effects from the boundaries were present during the simulations.

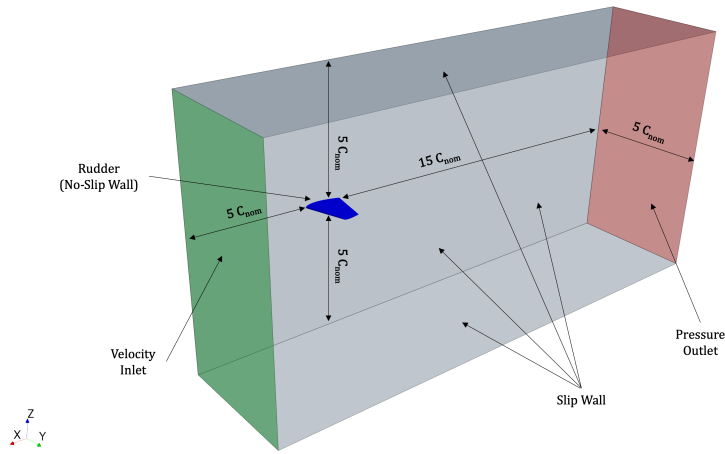


Figure 3. Computational domain sizing and boundary conditions.

3.3 Grid Generation

The computational domain was meshed using polyhedral cells. The boundary layer was resolved using prism layers tailored for the low y^+ wall treatment model with a target $y^+ < 1$. 18 prism layers were used, expanding with a growth ratio of ~ 1.4 . The prism layer mesh was extended onto an interface past the trailing edge into the core mesh, as otherwise it would have collapsed upstream from the sharp trailing edge due to the sharp TE angle which would have affected the resolving of the boundary layer. The final mesh for the highest lifting (and resulting highest suction side velocity) test case achieved $y_{avg}^+ \approx 0.68$ and a maximum $y_{max}^+ \approx 2.5$ on the LE. The volume mesh for one representative case is displayed in Fig. 4.

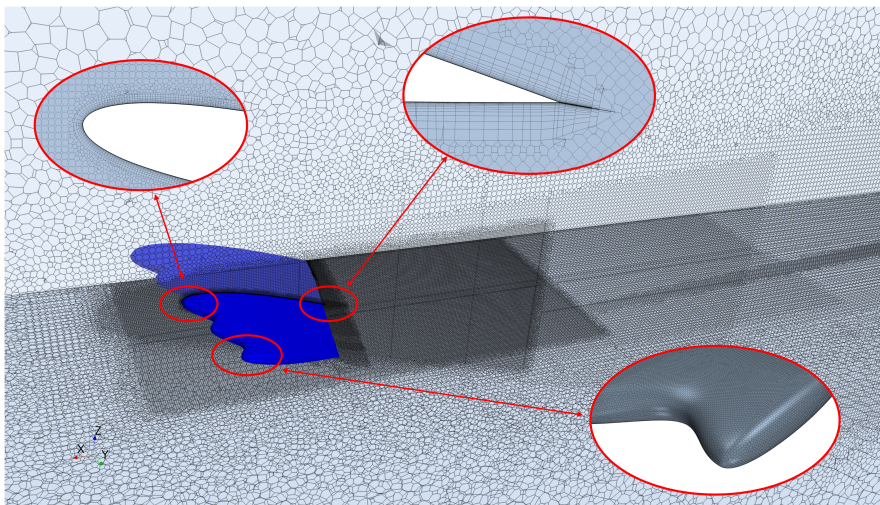


Figure 4. Volume mesh of the computational domain.

The rudder surface was meshed in a uniform manner and with a resolution as fine as feasible within the computational limits to accurately resolve the boundary layer where most of the vorticity of the turbulent wake is generated. Several mesh refinements were added in the vicinity of the rudder and in the downstream area to accurately resolve the turbulent wake. The tip vortex paths were estimated in preliminary simulations and additional refinements were added in its approximate trajectory.

An initial set of solutions was generated with a 11.3 million cell mesh (M_{11}). This setup however could not capture flow stall and the chaotic turbulent wake at high AOA with the desired accuracy. A second, much more refined grid with 21.6 million cells (M_{21}) was employed for stall and post-stall AOA.

3.4 Hydrodynamic Validation against Experimental Reference Study

The numerical lift and drag coefficient results, C_L and C_D respectively, for M_{11} and M_{21} from the reference rudder design were compared against the experimental data presented in Folger Whicker and Fehlner (1958). The coefficients are defined as follows:

$$C_L = \frac{2L}{\rho V^2 A_{lift}}, \quad (3)$$

$$C_D = \frac{2D}{\rho V^2 A_{lift}}, \quad (4)$$

where L and D are the lift and drag forces respectively, ρ is the fluid density, V is the free stream velocity, and A_{lift} is the lifting area defined as $S \times C_{nom}$. For the linear lifting regime of the reference rudder, AOA 5° , 10° , and 15° were chosen. C_{Lmax} is achieved at approximately 20° AOA and the data for the highest AOA in the reference study is provided for 21.5° where the rudder is stalled. Additionally, AOA of 25° and 30° were analysed for post-stall assessment, where the tubercles are expected to perform the best. The highest velocity test case for the reference rudder was selected with $R_n 2.26 \times 10^6$ based on C_{nom} . The validation results are shown in Fig. 5, the numerical values are averages of the statistically steady simulations.

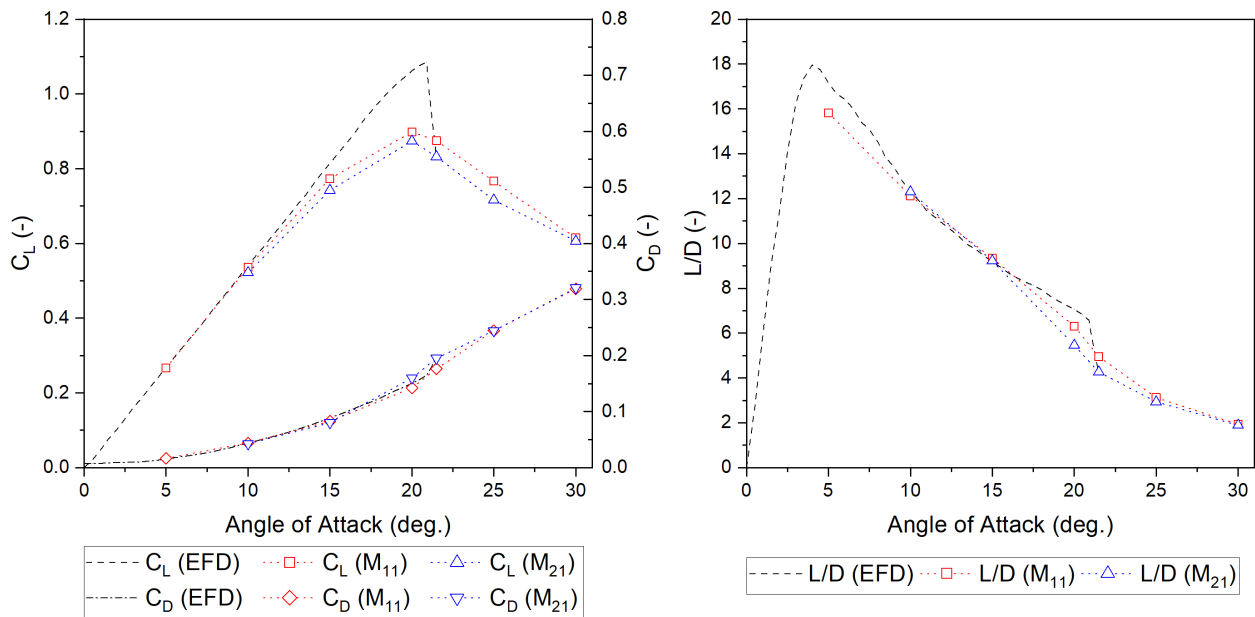


Figure 5. Validation of reference rudder force coefficients (left) and lift-to-drag ratio (right) for M_{11} and M_{21} against experimental results from Folger Whicker and Fehlner (1958) for $R_n 2.26 \times 10^6$.

The numerical results for C_L , C_D , and L/D are in good agreement with the experimental data, although C_{Lmax} is underpredicted. M_{11} failed to accurately predict flow separation at higher AOA, which was addressed through the introduction of the more refined M_{21} that accurately captured the separated wake structures. The results presented in the following section were generated with M_{11} for AOA 5° - 15° and with M_{21} for AOA 20° - 30° .

3.5 Grid Convergence Analysis

Additional verification is given for M_{11} at AOA 10° for pre-stall assessment and for M_{21} at AOA 21.5° for post-stall assessment by a Grid Convergence Index (GCI) analysis as outlined in Celik *et al.* (2008). GCI is a method based on Richardson extrapolation and compares the results of a critical variable (ϕ) for three

progressively refined meshes (N_i). The resultant GCI value states numerical uncertainty within the results progressing from a coarser to the next finer mesh. C_L and C_D were chosen as critical variables. The results of the GCI study are presented in Tab. 1. M_{11} converged monotonic and the GCI values for the fine grid of 1.5% and 2.1% were deemed sufficiently accurate. The convergence for the triplet of M_{21} is oscillatory, which further highlights the difficulties of numerical stall prediction. M_{21} is therefore judged based on its good agreement with the experimental results discussed in Section 3.4.

Table 1. Numerical uncertainty results for C_L and C_D .

AOA	φ	φ_1	φ_2	φ_3	N_1	N_2	N_3	GCI ₂₁	GCI ₃₂
M_{11} 10.0°	C_L	0.5365	0.5401	0.5446	11272268	4418389	1996886	1.465%	2.273%
	C_D	0.0443	0.0452	0.0470	11272268	4418389	1996886	2.097%	4.716%
M_{21} 21.5°	C_L	0.8323	0.8819	0.8271	21608805	9684232	3655372	Oscillatory convergence.	
	C_D	0.1952	0.1903	0.1951	21608805	9684232	3655372	Oscillatory convergence.	

4. RESULTS AND DISCUSSION

4.1 Force Coefficient Comparison

Force coefficient comparisons give a first indication of how the tubercle modifications affect the performance of the base rudder. The lift and drag coefficients and their ratio have been compared for the three rudder models, as presented in Fig. 6.

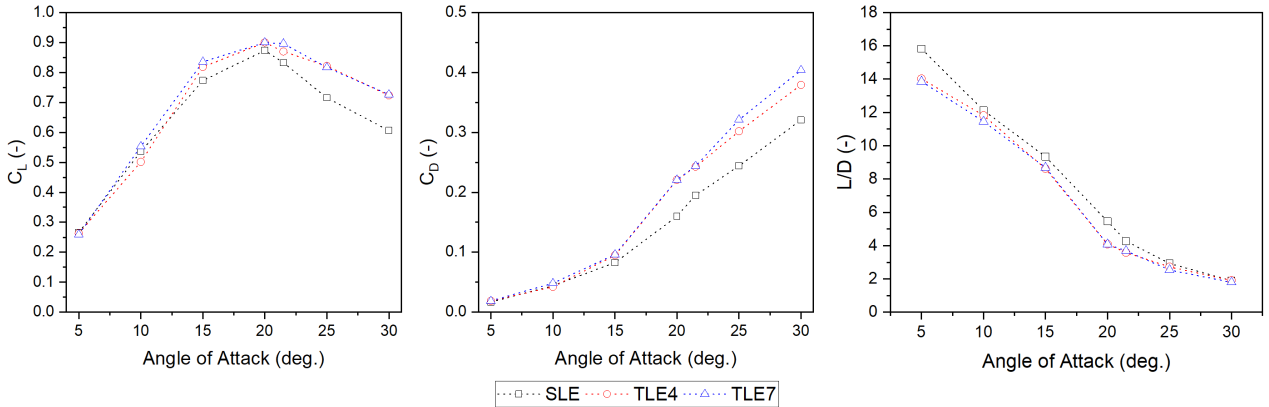


Figure 6. Force coefficient comparison between SLE, TLE4, and TLE7 at $R_n 2.26 \times 10^6$.

The tubercle modifications improved lift for AOA 15° and above, but also increased drag significantly leading to an overall reduction in L/D for all AOA considered. The most significant improvements in C_L were obtained at post-stall AOA 25° and 30° with enhancements of 14% and 19%, respectively. With both TLE rudders showing very similar post-stall lift, but TLE4 having a less significant drag penalty, TLE4 is regarded the more favourable modification. This is in line with the findings of Custodio *et al.* (2015); Weber *et al.* (2010) who reported that for a fixed amplitude, tubercles with larger wavelengths perform better. The general improvements in C_L suggest that the rudder effectiveness is increased by the tubercles, whereas due to the reduction in lift-to-drag ratio the modifications make the rudder less efficient.

4.2 Pressure Coefficient Comparison

The pressure coefficient, C_p , was visualised through isolines on the rudder suction side surface (Figs. 7, 8) and plotted for representative profile sections at several spanwise positions (Fig. 7 bottom row).

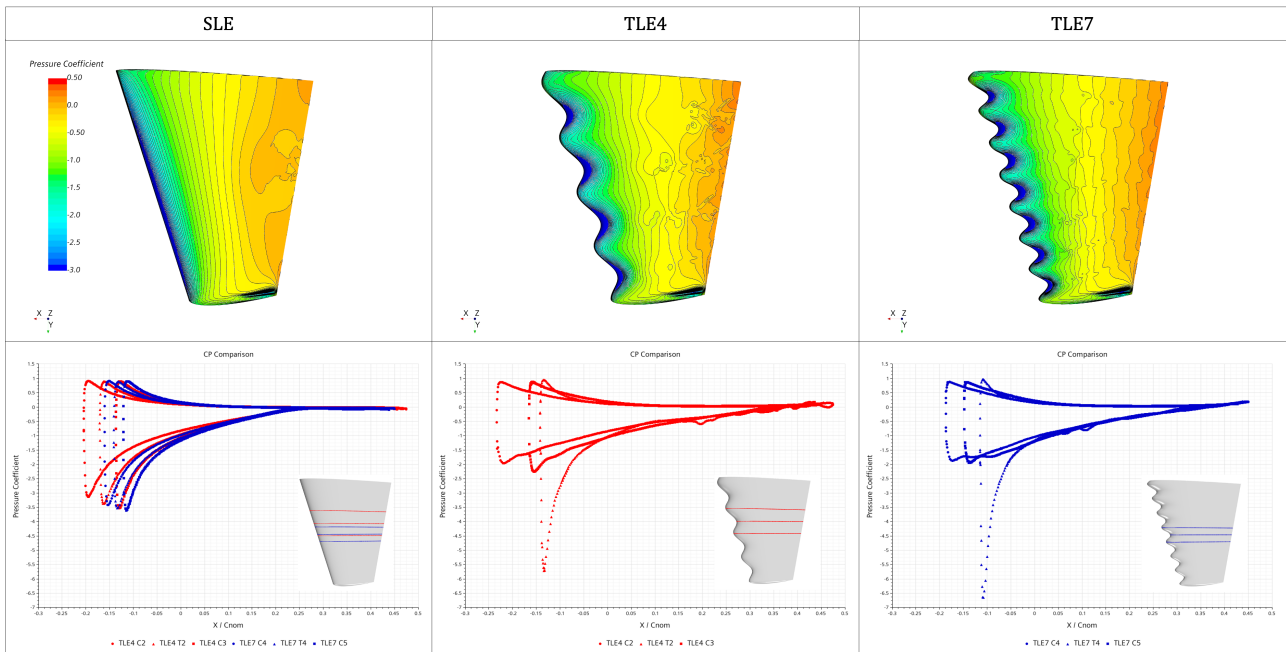


Figure 7. Pressure coefficient distribution comparison between SLE, TLE4, and TLE7 at AOA 15° (pre-stall) for rudder suction side (top row) and representative foil sections (bottom row), where C_n and T_n are the crest and trough sections of the TLE numbered from the root section outwards.

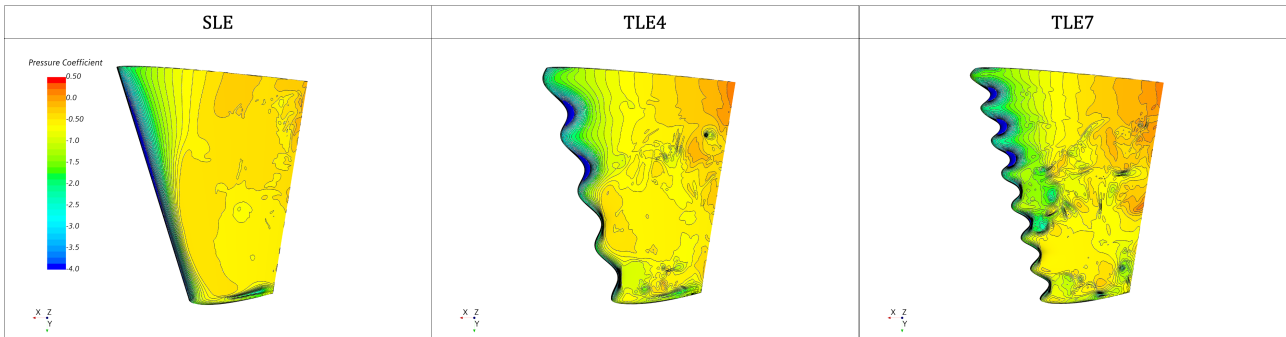


Figure 8. Pressure coefficient distribution comparison between SLE, TLE4, and TLE7 at AOA 21.5° (post-stall) for rudder suction side.

Fig. 7 shows how the tubercles introduce a strong spanwise pressure variation along the LE with strong low pressure peaks in the troughs and higher pressure areas over the crests. The low pressure in the tubercle troughs redirects the flow into the area between adjacent tubercles. The flow is forced around the tubercles, which has been reported to give rise to initial streamwise counter-rotating vorticity (Rostamzadeh et al., 2014). Comparing the C_p plots in Fig. 7, shows how the increased low pressure near the LE for the tubercle troughs results in a much larger adverse pressure gradient compared to the tubercle peak sections or the unmodified rudder sections. The larger adverse pressure gradient, combined with the reduced chord length of the trough sections causes early flow separation downstream from the troughs. The opposite effect holds true for the crests, where the flow attachment is prolonged.

The spanwise pressure variation is maintained over the majority of the suction side surface, which supports the argument of flow compartmentalisation generated by the tubercles that allows them to limit the spanwise

progression of flow separation (Bolzon et al., 2015; Pedro and Kobayashi, 2008). At AOA 15° (Fig. 7) the SLE shows onsets of flow separation spread across the entire TE area, for post-stall AOA 21.5° (Fig. 8) the C_p contours are closely gathered near the LE with a neutral C_p spread over the whole span of the surface indicating that the flow has separated. For TLE4 at AOA 15° separation appears confined into several pockets downstream from the troughs at the TE, for TLE7 the flow separates intermittently on the TE only. At AOA 21.5° both tubercle rudders also show larger areas of separated flow. However these separation areas appear concentrated to the mid-sections (TLE4) and tip sections (TLE7), with strong tubercle effects and attached flow at the root.

4.3 Streamwise Counter-Rotating Vortex Formation and Near-Field Interaction

Whenever two or more vortices flow in parallel at a sufficiently close separation distance their strain fields begin to influence each other which causes two-dimensional and three-dimensional vortex interaction. Leweke *et al.* (2016) present a comprehensive summary of the different interaction mechanisms, many of which occur within the wake downstream from the tubercle rudders as will be discussed in the following section. To analyse the flow dynamics in the wake, cut-planes normal to the free stream with scalar displayers for stream-wise vorticity were defined. Positive vorticity is rotating in clockwise direction (coloured red), negative vorticity in the anti-clockwise direction (coloured blue) about the positive x-axis. The visualisations of the instantaneous flow field for the three rudders at AOA 10° , 15° , and 20.0° can be seen in Figs. 9-11. For simplification individual tubercle crests and troughs are numbered as C_1 to C_n and T_1 to T_n , respectively, where C_1 and T_1 are the crest and trough closest to the root of the rudder.

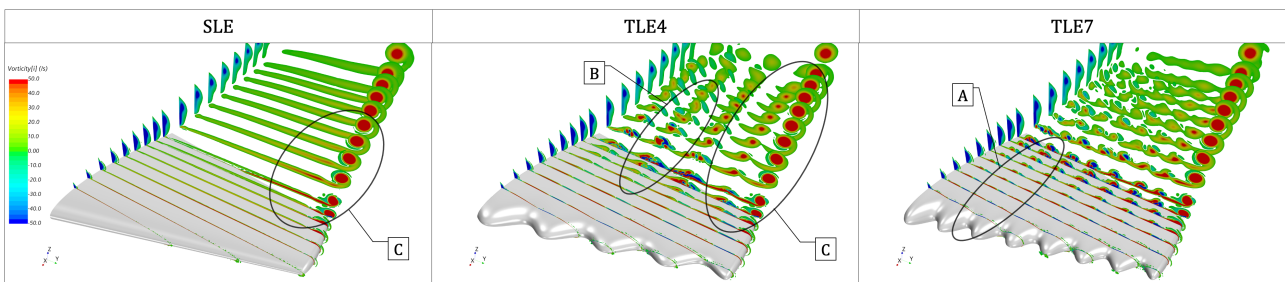


Figure 9. Isosurface visualisation of streamwise vorticity for SLE, TLE4 and TLE7 at AOA 10° .

In Fig. 9, at the low AOA of 10° where the flow is largely attached, the flow profiles for the SLE and TLE are fundamentally different. The SLE rudder shows positive vorticity over most of the suction side surface, indicative of the spanwise flow component inherent in finite span foils. Downstream this vorticity forms a typical vortex sheet which is rolling up into the tip vortex.

Over each tubercle positive vorticity is generated from the tip-facing side and negative vorticity from the root-facing side. This is the initial stream-wise counterrotating vorticity resulting from the spanwise pressure variations diverting the flow into the troughs. The circulation of these vortices increases with chordwise distance behind the troughs, as can be seen in Area A in Fig. 9. One key characteristic of the TLE is the early flow separation behind the troughs where small stall cells form. The streamwise vorticity is strengthened significantly on either side of these stall cells. This has been explained in detail by Hansen *et al.* (2016) and Rostamzadeh *et al.* (2014) for infinite-span foils and the observations from this study suggest that the principal vortex generating mechanism is the same. However there some key variations as a result of the finite-span nature of the rudder. The flow spilling over from the pressure side to the suction side over the tip causes tubercle vortex generation of unequal strength and size. The negative vorticity is generated against the spanwise flow direction which limits the build-up, whereas the positive vorticity is enhanced. Generally, as AOA is increased, tubercle vortex strength also increases.

A strong interaction among the tubercle vortices themselves exists. Area B in Fig. 9 shows how the weaker negative (blue) tubercle vortex starts circling around the stronger positive vortex and is annihilated in the process. This effect is present for all tubercle vortex pairs and is more pronounced in the tip areas where the spanwise flow is stronger, annihilating negative (blue) tubercle vorticity shortly downstream from the TE. The

positive (red) tubercle vortices however remain persistent in the flow up to a distance of $2\sim 3 C_{nom}$ downstream from the TE. A particularly strong secondary vortex is generated close to the tip vortex by TLE4 C_4 and TLE7 C_7 .

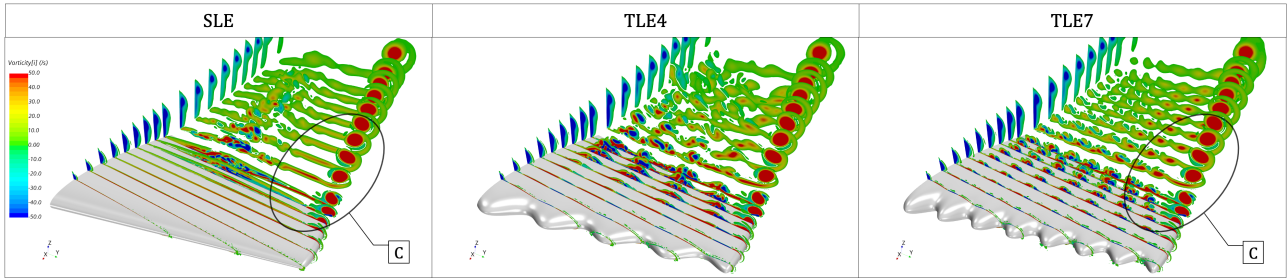


Figure 10. Isosurface visualisation of streamwise vorticity for SLE, TLE4 and TLE7 at AOA 15° .

The presence of these vortices in the flow field causes a significant interruption of vortex sheet behind the TE, which can be seen when comparing Areas C in Figs. 9-10. At AOA 10° (Fig. 9) the positive tubercle vortices from TLE4 introduce spanwise separations within the vortex sheet. The tubercle vortices dissipate part of the vorticity that is generated when the pressure difference between pressure and suction side is balanced out at the TE. As a result the circulation around the tip vortex for TLE4 is reduced. A similar effect can be seen for TLE7 at AOA 15° (Fig. 10), when the smaller tubercles of this rudder begin to generate stronger vorticity. TLE7 also creates strong flow compartmentalisation which may explain the increase in C_L as a result of an induced drag reduction. The spanwise flow component causes vortex pairs close to the tip to turn towards the root to a certain degree. As soon as these vortices detach from the surface and stream past the TE, the strain field from the tip vortex changes their trajectory and they are turned outwards. Partial merging with the tip vortex can be seen.

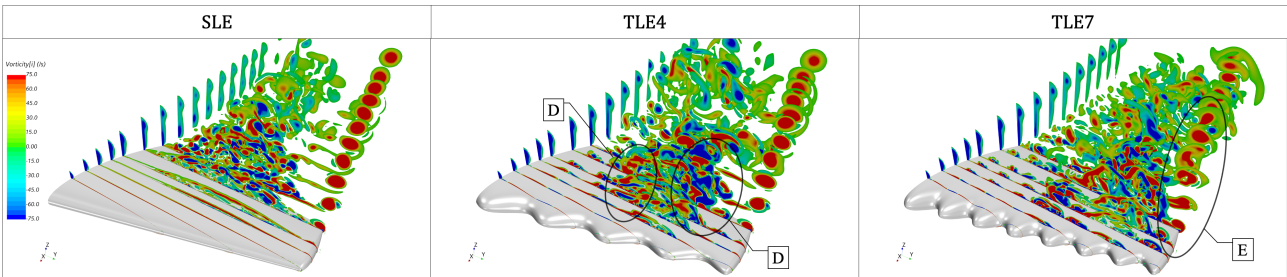


Figure 11. Isosurface visualisation of streamwise vorticity for SLE, TLE4 and TLE7 at AOA 20° .

Fig. 11 shows the three rudders for AOA 20° close to stall. Significant differences in the separation behaviour between the SLE rudder and the two TLE rudders can be seen. On the SLE rudder formation of a stall cell begins centralised on along the TE (see Fig. 10) from where it rapidly spreads across the entire span and towards the LE (see Fig. 11). As discussed, the modification of the surface pressure from the tubercles together with the boundary layer momentum exchange from the streamwise vortex pairs leads to early separation in the trough areas and maintained flow attachment over the crests (see Fig. 10). As AOA increases the stall cells behind each trough may spread out and combine, but generally remain confined between a few tubercles and do not spread out across the entire span. Strong tubercle vortex pairs develop for $T_{1,2}$ and T_{1-3} of TLE4 and TLE7, respectively. The streamwise vortices in this area appear to strongly energise the boundary layer resulting in very little separated flow and giving a 3% increase in C_L over the SLE rudder. For TLE4 the stall cell is confined in between C_2 and C_4 . For TLE7, flow separation is confined outwards from C_4 but expands to the rudder tip. Rostamzadeh *et al.* (2017) showed that similarly to the small separation cells behind the tubercle troughs which strengthen the streamwise vortex formation for individual pairs, large structures of streamwise vorticity of opposing signs form either side of the larger stall cells. This effect is very evident for both, TLE4 and TLE7 (e.g. Area D in Fig.11).

The strong separation in the tip region of TLE7 furthermore has a tip-offloading effect which has a strong impact on the tip vortex. Whilst the tip vortex for the SLE has a very clearly defined strong vortex core with a straight trajectory, the tip vortex for TLE7 is heavily distorted, showing signs of elliptic flow within the core, diffusion, as well as potential long-wave instabilities in its path (see Area E in Fig. 11). Less vorticity is generated as a result from the tip offloading and further weakening stems from interaction with the negative vorticity generated around the stall cell. Whilst the impact on the tip vortex of TLE4 is not as significant, there are still signs of elliptic flow in the core sections, as well as a distortion to its trajectory through Crow and/or elliptic instabilities.

4.5 Effects of TLE on Turbulent Wake and Tip Vortex Decay

A significantly different flow separation pattern between the models and vortex interaction effects between the tubercle vortices and the tip vortex, especially for TLE7, has been identified for AOA 20°. The following section gives a closer insight for this angle and the stall angle AOA 21.5°. The vortical wake structures were visualised using Q-criterion isosurface with $Q = 100.0/s^2$. To give an insight into the relative strength of the wake and its features, the turbulent kinetic energy (TKE) is displayed on the isosurface. A vertical plane view facing the root (top) and a horizontal plane view facing the suction side (bottom), showing the instantaneous flow field are presented for each rudder configuration for AOA 20° and 21.5° in Fig. 12.

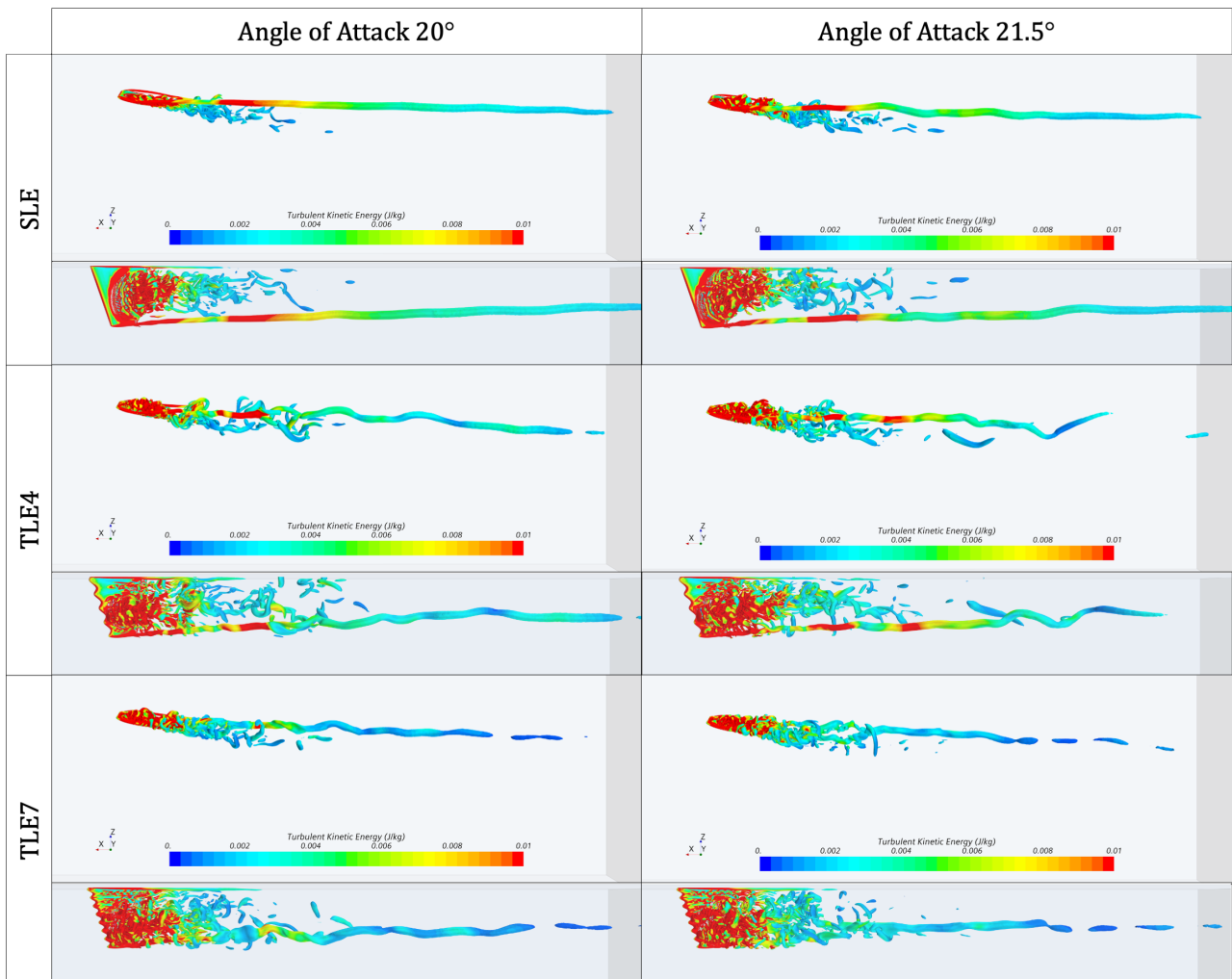


Figure 12. Turbulent kinetic energy visualised on Q-criterion isosurface for SLE, TLE4, and TLE7 at AOA 20° (left) and AOA 21.5° (right).

At AOA 20° the SLE rudder develops a strong coherent tip vortex that streams in a straight line. For TLE4 there is an initial interference with the large negative vortical structure, shown in Area D of Fig. 11, giving rise to initial short-wave elliptical instabilities. Large elements of positive vorticity generated by the tubercles remain persistent within the turbulent wake and begin interacting with the tip vortex several chord lengths downstream. The stronger co-rotating tip vortex core causes these elements to circulate around it as they dissipate. In the process the tip vortex begins to show long-wave instabilities, clearly visible in the vertical plane. Overall TKE within the core appears to be reduced compared to the SLE and it dissipates further upstream.

For TLE7 the confined separation in the tip area can be seen, which causes the offloading the rudder tip that initially reduces vortex strength. The larger negative vortical structure forming around the stall cell is located closely to the tip vortex. Long-wave Crow instabilities become visible within the tip vortex as the counter-rotating negative vortex is bent into vortex rings around it. The initially weakened tip vortex experiences a second interaction with the positive, co-rotating vortex generated around the root side of the stall cell approximately 2 chord lengths downstream. The difference in strength of these two vortices is smaller, causing them to merge in a spiralling motion throughout which the tip vortex core strength is reduced but its circulation is increased. Out of the three rudders, TLE7 has the fastest tip vortex dissipation.

At AOA 21.5° the SLE rudder is stalled. Flow separation across the full span extending up to the LE, as well as large vortical elements being shed several chord lengths into the wake behind the rudder can be seen. Still, a fully developed tip vortex, is generated. At this angle the TLE rudders begin to produce significantly more lift. Naturally, one would therefore expect a stronger tip vortex generation from the TLE rudders, however this is not the case. The main effects discussed for AOA 20° persist and the tip vortex is distorted. Extended separation further across the span for TLE4 leads to a larger turbulent wake formation in the near-field. The increased wake sheds stronger vortical elements that begin to spiral in the strain field of the tip vortex and induce instabilities that accelerate the decay. For TLE7, the flow separation spreads out further, with the stall cell beginning in T_3 . The full separation of the flow in the tip area leads to the formation of a very weak tip vortex extending from the general wake. The vortex follows a straight line trajectory, however the interaction with vortical elements in the wake upstream causes it to be displaced inwards in-line with C_6 and dissipates quickly.

The tip vortices are generally weakened for the TLE due to interaction with the stall cell that has been shifted outwards as a result of the compartmentalisation from the tubercle vortices. Whilst the separation is more confined, it is more chaotic and energetic in itself. The vertical plan views in Fig. 14 show an increase in volume of the vortical structures in the near-field wake, which also appear to contain higher TKE levels, especially in the case of TLE7. This results in the drag penalty reported for the tubercles, which becomes severe from AOA 20° upwards.

5. CONCLUSIONS

A representative marine rudder and two tubercle leading edge modifications were analysed numerically using DES. The three models were tested over a wide range of angles of attack from 5° to 30° at a Reynolds number of 2.26×10^6 . The lifting performance was compared through lift and drag coefficient measurements. The main focus of the presented work was the effect of the TLE modification on the downstream turbulent wake structure with particular focus on the tip vortex development. The analysis was conducted through visualisations of streamwise vorticity and q-criterion isosurface with turbulent kinetic energy. The following conclusions can be drawn:

1. The formation of streamwise counter-rotating vortex pairs behind the tubercles was shown. Spanwise flow effects caused the vortices generated to be of unequal strength. The negative vortices were annihilated by their positive counter-pairs, especially close to the rudder tip. The positive tubercle vortices remained persistent within the flow up to $3 C_{nom}$ downstream from the TE. At low AOA, the tubercle vortices broke up the vortex sheet by dissipating its energy and in turn minimising the circulation of the tip vortex.

2. At higher AOA the TLE modifications changed the flow separation on the rudder suction side through flow compartmentalisation. Separation for the SLE rudder began centralised on the TE and spread out across the entire span. TLE4 confined flow separation centralised between tubercles C_2 and C_4 . TLE7 confined separation outwards from C_4 resulting in an offloading of the tip. The tip vortex strength of TLE7 was reduced significantly and it decayed at a shorter distance downstream. Vortical elements of counter-rotating vorticity were generated on either side of the stall cell of each TLE rudder. Interaction of this vorticity with the tip vortex had weakening effects and displaced the tip vortex in its trajectory.
3. The tubercles caused early flow separation in the troughs. This separation paired with the tubercle vortex structures increased the turbulent wake strength and size in the near field behind the rudder causing a large drag penalty which compromised the TLE rudders' efficiency. However lift from the TLE rudders was increased for almost the entire AOA range, most significantly in the post-stall regime, making the rudders more effective.
4. Out of the two tubercle modifications the longer wavelength of TLE4 provided better lifting performance, but TLE7 had the most significant impact on the tip vortex generation, distorting its trajectory and largely accelerating decay.

ACKNOWLEDGEMENTS

The results were obtained using the University of Strathclyde's High Performance Computer ARCHIE-WeSt (<https://www.archie-west.ac.uk/>). This work was supported by the Royal Society (Ref: RGS\R1\191167) and BAE systems plc. (Ref: MEIR PhD 17), which is greatly appreciated and acknowledged.

REFERENCES

- Bolzon, M.D., Kelso, R.M., Arjomandi, M., 2017. Performance effects of a single tubercle terminating at a swept wing's tip. *Exp. Therm. Fluid Sci.* 85, 52–68. <https://doi.org/10.1016/j.expthermflusci.2017.02.016>
- Bolzon, M.D., Kelso, R.M., Arjomandi, M., 2015. Tubercles and Their Applications. *J. Aerosp. Eng.* 29, 1–10. [https://doi.org/10.1061/\(ASCE\)AS.1943-5525](https://doi.org/10.1061/(ASCE)AS.1943-5525)
- Câmara, J.F.D., Sousa, J.M.M., 2013. Numerical Study on the Use of a Sinusoidal Leading Edge for Passive Stall Control at Low Reynolds Number, in: 51st AIAA Aerospace Sciences Meeting Including the New Horizons Forum and Aerospace Exposition 2013. American Institute of Aeronautics and Astronautics, Dallas, Texas, US. <https://doi.org/10.2514/6.2013-62>
- Carrica, P.M., Kim, Y., Martin, J.E., 2019. Near-surface self propulsion of a generic submarine in calm water and waves. *Ocean Eng.* 183, 87–105. <https://doi.org/10.1016/j.oceaneng.2019.04.082>
- Celik, I.B., Ghia, U., Roache, P.J., Freitas, C.J., Coleman, H., Raad, P.E., 2008. Procedure for Estimation and Reporting of Uncertainty Due to Discretization in CFD Applications. *J. Fluids Eng. Trans. ASME* 130. <https://doi.org/10.1115/1.2960953>
- Custodio, D., 2012. The Effect of Humpback Whale-Like Leading Edge Protuberances. Worcester Polytechnic Institute.
- Custodio, D., Henoach, C.W., Johari, H., 2015. Aerodynamic Characteristics of Finite Span Wings with Leading-Edge Protuberances. *AIAA J.* 53. <https://doi.org/10.2514/1.J053568>
- Fish, F.E., Battle, J.M., 1995. Hydrodynamic Design of the Humpback Whale Flipper. *J. Morphol.* 225, 51–60. <https://doi.org/10.1002/jmor.1052250105>

- Fish, F.E., Howle, L.E., Murray, M.M., 2008. Hydrodynamic flow control in marine mammals. *Integr. Comp. Biol.* 48. <https://doi.org/10.1093/icb/icn029>
- Folger Whicker, L., Fehlner, L.F., 1958. *Free-Stream Characteristics of a Family of Low-Aspect-Ratio, All-Movable Control Surfaces for Application to Ship Design.* Washington, D.C.
- Hansen, K.L., Rostamzadeh, N., Kelso, R.M., Dally, B.B., 2016. Evolution of the streamwise vortices generated between leading edge tubercles. *J. Fluid Mech.* 788, 730–766. <https://doi.org/10.1017/jfm.2015.611>
- Johari, H., 2015. Cavitation on hydrofoils with sinusoidal leading edge, in: *Journal of Physics: Conference Series - 9th International Symposium on Cavitation (CAV2015).* IOP Publishing. <https://doi.org/10.1088/1742-6596/656/1/012155>
- Knister, D., Callison, E., Ganesh, H., Ceccio, S.L., Arbor, A., 2020. Experimental Study of Cavitation Inception During the Interaction of Vortices, in: *33rd Symposium on Naval Hydrodynamics.* Osaka, Japan.
- Leweke, T., Le Dizès, S., Williamson, C.H.K., 2016. Dynamics and Instabilities of Vortex Pairs. *Annu. Rev. Fluid Mech.* 48, 507–541. <https://doi.org/10.1146/annurev-fluid-122414-034558>
- Liu, J., Hekkenberg, R., 2017. Sixty years of research on ship rudders: effects of design choices on rudder performance. *Ships Offshore Struct.* 12, 495–512. <https://doi.org/10.1080/17445302.2016.1178205>
- Malipeddi, A.K., Mahmoudnejad, N., Hoffmann, K.A., 2012. Numerical Analysis of Effects of Leading-Edge Protuberances on Aircraft Wing Performance. *J. Aircr.* 49, 1336–1344. <https://doi.org/10.2514/1.C031670>
- Miklosovic, D.S., Murray, M.M., Howle, L.E., 2007. Experimental Evaluation of Sinusoidal Leading Edges. *J. Aircr.* 44, 1404–1408. <https://doi.org/10.2514/1.30303>
- Miklosovic, D.S., Murray, M.M., Howle, L.E., Fish, F.E., 2004. Leading-edge tubercles delay stall on humpback whale (*Megaptera novaeangliae*) flippers. *Phys. Fluids* 16, L39–L42. <https://doi.org/10.1063/1.1688341>
- Molland, A.F., Turnock, S.R., 2007. *Marine Rudders and Control Surfaces: Principles, Data, Design and Applications.* Elsevier/Butterworth-Heinemann.
- Pedro, H.T.C., Kobayashi, M.H., 2008. Numerical Study of stall delay on humpback whale Flippers, in: *46th AIAA Aerospace Sciences Meeting and Exhibit.* American Institute of Aeronautics and Astronautics, Reno, Nevada, US. <https://doi.org/10.2514/6.2008-584>
- Rostamzadeh, N., Hansen, K.L., Kelso, R.M., Dally, B.B., 2014. The formation mechanism and impact of streamwise vortices on NACA 0021 airfoil's performance with undulating leading edge modification. *Phys. Fluids* 26, 1–22. <https://doi.org/10.1063/1.4896748>
- Rostamzadeh, N., Kelso, R.M., Dally, B., 2017. A numerical investigation into the effects of Reynolds number on the flow mechanism induced by a tubercled leading edge. *Theor. Comput. Fluid Dyn.* 31. <https://doi.org/10.1007/s00162-016-0393-x>
- Shanmukha Srinivas, K., Datta, A., Bhattacharyya, A., Kumar, S., 2018. Free-stream characteristics of bio-inspired marine rudders with different leading-edge configurations. *Ocean Eng.* 170, 148–159. <https://doi.org/10.1016/j.oceaneng.2018.10.010>

- Shi, W., Atlar, M., Norman, R., Aktas, B., Turkmen, S., 2016. Numerical optimization and experimental validation for a tidal turbine blade with leading-edge tubercles. *Renew. Energy* 96, 42–55. <https://doi.org/10.1016/j.renene.2016.04.064>
- Spalart, P.R., 2001. *Young-Person's Guide to Detached-Eddy Simulation Grids*. Hampton, Virginia, US.
- Stanway, M.J., 2008. Hydrodynamic effects of leading-edge tubercles on control surfaces and in flapping foil propulsion. Massachusetts Institute of Technology, Massachusetts Institute of Technology.
- Weber, P.W., Howle, L.E., Murray, M.M., 2010. Lift, Drag, and Cavitation Onset On Rudders With Leading-edge Tubercles. *Mar. Technol.* 47, 27–36. <https://doi.org/10.5957/mtsn.2010.47.1.27>
- Yoon, H.S., Hung, P.A., Jung, J.H., Kim, M.C., 2011. Effect of the wavy leading edge on hydrodynamic characteristics for flow around low aspect ratio wing. *Comput. Fluids* 276–289. <https://doi.org/10.1016/j.compfluid.2011.06.010>